AFRL-RX-WP-TP-2012-0371

PHASE TRANSFORMATIONS IN THE OXYGEN-ENRICHED CASE LAYER OF BETA TITANIUM ALLOYS FORMED DURING OXIDATION (PREPRINT)

J. Tiley
Metals Branch
Structural Materials Division

A. Behera, K. Mahdak, H. Mohseni, S. Nag, and R. Banerjee
University of North Texas

August 2012
Interim

AIR FORCE RESEARCH LABORATORY
MATERIALS AND MANUFACTURING DIRECTORATE
WRIGHT-PATTERSON AIR FORCE BASE, OH 45433-7750
AIR FORCE MATERIEL COMMAND
UNITED STATES AIR FORCE

REPORT DOCUMENTATION PAGE

Form Approved
OMB No. 0704-0188

1. REPORT DATE *(DD-MM-YY)*	2. REPORT TYPE	3. DATES COVERED *(From - To)*
August 2012	Technical Paper	1 July 2012 – 1 August 2012

4. TITLE AND SUBTITLE
PHASE TRANSFORMATIONS IN THE OXYGEN-ENRICHED CASE LAYER OF BETA TITANIUM ALLOYS FORMED DURING OXIDATION (PREPRINT)

5a. CONTRACT NUMBER
FA8650-08-C-5226

5b. GRANT NUMBER

5c. PROGRAM ELEMENT NUMBER
62102F

6. AUTHOR(S)
J. Tiley (RXCM)
S. Nag, and R. Banerjee, A. Behera, K. Mahdak, and H. Mohseni (University of North Texas)

5d. PROJECT NUMBER
4347

5e. TASK NUMBER

5f. WORK UNIT NUMBER
LM114100

7. PERFORMING ORGANIZATION NAME(S) AND ADDRESS(ES)
University of North Texas
Corner of Avenue C Chestnut
Denton, TX 76203

8. PERFORMING ORGANIZATION REPORT NUMBER

9. SPONSORING/MONITORING AGENCY NAME(S) AND ADDRESS(ES)
Air Force Research Laboratory
Materials and Manufacturing Directorate
Wright-Patterson Air Force Base, OH 45433-7750
Air Force Materiel Command
United States Air Force

10. SPONSORING/MONITORING AGENCY ACRONYM(S)
AFRL/RXCM

11. SPONSORING/MONITORING AGENCY REPORT NUMBER(S)
AFRL-RX-WP-TP-2012-0371

12. DISTRIBUTION/AVAILABILITY STATEMENT
Approved for public release; distribution unlimited. Preprint to be submitted to Scripta Materialia.

13. SUPPLEMENTARY NOTES
The U.S. Government is joint author of this work and has the right to use, modify, reproduce, release, perform, display, or disclose the work. PA Case Number and clearance date: 88ABW-2012-2672, 8 May 2012. This document contains color.

14. ABSTRACT
The formation of an oxide layer along together with α precipitation in the subsurface oxygenenriched zone, during the oxidation of a β-Ti alloy, has been investigated using SEM, (S)TEM, and nanoindentation. Just below the nanocrystalline oxide layer, a two-phase mixture consisting of nanoscale equiaxed α grains and rutile grains is formed. Further below, the morphology of the α precipitates transitions to more lath-like with their size-scale, nucleation density, and the volume fraction of β progressively changing with increasing depth.

15. SUBJECT TERMS
Beta 21s, oxidation, titanium alloys, oxygen, nano indentation, hardness, case layer

16. SECURITY CLASSIFICATION OF:			17. LIMITATION OF ABSTRACT:	NUMBER OF PAGES	19a. NAME OF RESPONSIBLE PERSON (Monitor)
a. REPORT	b. ABSTRACT	c. THIS PAGE			Jaimie Tiley
Unclassified	Unclassified	Unclassified	SAR	16	19b. TELEPHONE NUMBER *(Include Area Code)* N/A

Phase transformations in the oxygen-enriched case layer of beta titanium alloys formed during oxidation

A. Behera, S. Nag, K. Mahdak, H. Mohseni, J. Tiley* and R. Banerjee

Center for Advanced Research and Technology, Department of Materials Science and Engineering, University of North Texas, Denton, Texas 76203, U. S. A.

*Materials and Manufacturing Directorate, Air Force Research Laboratory, Dayton, Ohio 45309, U. S. A.

Abstract

The formation of an oxide layer along together with α precipitation in the subsurface oxygen-enriched zone, during the oxidation of a β-Ti alloy, has been investigated using SEM, (S)TEM, and nanoindentation. Just below the nanocrystalline oxide layer, a two-phase mixture consisting of nanoscale equiaxed α grains and rutile grains is formed. Further below, the morphology of the α precipitates transitions to more lath-like with their size-scale, nucleation density, and the volume fraction of β progressively changing with increasing depth.

Keywords- Beta 21s, oxidation, titanium alloys, oxygen, nano indentation, hardness, case layer

Paper

In recent years, there has been an increased interest in the use and further development of several β titanium alloys for high temperature aerospace applications. Apart from cold formability and age hardening characteristics, these metastable β alloys have improved formability and are capable of higher strength and toughness [1-3]. The balance of mechanical properties is expected to be dependent on the volume fraction, size, morphology and distribution of α precipitates within the β matrix [4,5]. However, these β titanium alloys suffer from poor elevated temperature properties, especially oxidation resistance. In addition to the oxide layer, the mechanism and kinetics of formation of an oxygen-enriched α case layer during the oxidation of these alloys play a critical role in limiting their application temperature. Timetal 21s (also known as Beta 21s [6]) has shown great promise in this respect due to its excellent high temperature corrosion and oxidation resistance [7]. Additional properties like age hardenability and ease of cold rolling and strip producing add to its superiority. It has also been characterized as having resistance to hot, reducing acid environments equivalent to that of grade 7 Titanium [8]. Studies on this alloy have mostly focused on its mechanical and environmental properties [7, 8], although some work has been done regarding on the microstructural evolution when subjected to numerous heat treatments [9]. In terms of oxidation studies on Beta 21s, the surface oxide layer was found to be a combination of TiO_2 and Al_2O_3, governed primarily by rate of diffusion of oxygen and the chemical reaction for oxide formation [10]. Oxygen, known to be a α stabilizer, is thereby assumed to be the reason for similar gradient in α precipitation, as reported by Wallace et. al. [11]. The current study complements the previous research in understanding how oxygen influences the formation of α case layer as well as the precipitation of fine-scale α within the β matrix of this alloy. The work pertains to the study of microstructure-property relationship from the oxide and oxygen-rich α layers in to the bulk microstructure, by coupling various

characterization techniques like scanning electron microscopy (SEM) and transmission electron microscopy (TEM) with nanoindentation measurements.

Thin plates of Beta 21s were subjected to open air oxidation heat treatments at temperature of 650^{O}C for duration of 50hrs. Prior to oxidation the samples were beta solutionized at 1000^{O}C (above the β transus temperature, 800-840^{O}C [8]) for 30 minutes followed by water quenching. Cross sectional specimens prepared from the oxidized plates were investigated in detail using scanning electron microscopy (SEM) carried out in a FEI Sirion™ FEG instrument operating at 30 keV. Specimens for transmission electron microscopy were prepared using a dual-beam focused ion beam (FIB), specifically the FEI Nova Nanolab 200 system. These were subsequently analyzed in a FEI Tecnai F20-FEG TEM where both diffraction and well as analytical studies (STEM-EDS) were conducted. Nanoindentation studies were conducted using a Nanoindenter XP system from MTS instruments.

Fig. 1(a) shows a secondary electron image of the oxidized Beta 21s sample where the brighter region on the right of the figure shows the oxide layer. Also due to the cross-sectional nature of the sample, one would imagine that the oxygen content in the alloy would decrease consistently from this oxide layer on the right to the base alloy on the left. From Fig. 1(a), a variation in the size-scale and nucleation density of the α precipitates is also observed with distance from the oxide-alloy interface. The larger scale alpha plates or laths are seen towards the left of this image, representing the bulk microstructure, while the size decreases to seemingly submicron range near the oxide interface. In Fig. 1(a) a plot showing the variation of oxygen counts (measured by Energy dispersive spectroscopy (EDS)) with distance from the top surface of the oxidized sample has been superimposed on the SEM

micrograph. As expected, the graph shows higher amounts of oxygen count in the oxide region on the right (top of the oxidized sample). As one probes from right to left (i.e. goes deeper into the sample) there is a steady decrease in oxygen counts that flattens out at ~10mm from the oxide/metal interface. From Fig. 1(a) if one tries to correlate between the size scale of α precipitates at a particular region of the sample with its oxygen content, it would be evident that higher oxygen content leads to more refined α precipitation. This may be due to higher availability of nucleation sites because of elevated amounts of interstitial oxygen in regions close to the oxide/metal interface. Although some speculations have been made in the past to determine the influence of interstitial elements like C and O on α nucleation sites and transformation kinetics [12, 13], more detailed investigations are required in this aspect and are currently underway.

Fig. 1(b) shows a high magnification secondary electron image of the oxidized Beta 21s sample. The figure also shows two different rows of nano-indents that are inclined at an angle of ~10º with the surface of the sample. Several such rows of indents were made at varying distances, ranging from 5 μm to 45 μm, from the oxide-alloy interface. The spacing between two successive indents was set at 10 μm. From fig. 1(b) the approximate size of these indents could be estimated as 3-4 μm. A plot of the hardness values obtained from these indents as a function of distance from the oxide-alloy interface has also been superimposed in fig. 1(b). This curve shows higher hardness values near the oxide layer, where finer α precipitates are present, as opposed the values obtained far into the bulk of the specimen. For example the indentation that was made 5 μm from the oxide-alloy interface gave a hardness reading of ~8.5 GPa while the hardness value obtained from an indent made 45 μm from this interface was ~5GPa. This shows that the variation in α precipitate size directly affects the mechanical

properties, with finer α resulting in higher hardness values. This is similar to the results obtained by previous researchers where the mechanical property values such as micro hardness and tensile strength of the alloy seemed to vary with its oxygen content [10, 14]. In order to further study the different zones that are formed during oxidation of Beta 21s, samples for transmission electron microscopy was prepared and analyzed.

Fig. 2(a) shows a scanning transmission electron microscopy (STEM) image that illustrates the change in microstructure, starting from the oxide layer (marked as 1) on the top to about 15 μm deep into the specimen. The grayish region above the oxide layer is the protective Pt coating that was deposited while making the TEM sample. This was done to prevent damage to the oxide and oxygen enriched layers during high kV Ga ion milling, a necessary step while preparing FIB based TEM samples. Despite all efforts, the difference in milling nature among the different oxide and oxygen-enriched layers present in the sample may cause some curtaining effects. This can be seen in the STEM image as black striations. Apart from that, based on the different microstructures that are visible in the TEM sample shown in fig. 2(a), the entire oxidized sample can be roughly divided into 4 distinct layers. Thus the region right below the oxide layer (1) contains very fine scale distribution of equiaxed α precipitates along with some oxide grains, marked as layer 2. This is distinctly different from layers 3 and 4 where the α precipitates seem exhibit a more plate-like or lath-like morphologies. However, the size scale of α laths in layer 3 is quite small (~50-100 nm). As one probes deeper into the sample, the α lath size increases consistently. Thus in layer 4, which represents the bulk microstructure, the α laths are ~2-3 μm in length. Further detailed TEM investigations of the oxide and oxygen enriched regions (layers 1 and 2 respectively) have been carried out. A bright field TEM micrograph of layer 1 (Fig. 2(b)) shows a large number

of nanocrystalline oxide grains, with an average grain size of ~20nm. The random orientation of these grains is clearly evident from the rings that are present in the selected area diffraction (SAD) pattern shown as an inset in fig. 2(b). For phase identification, the "d" spacing of these rings were compared with the ICDD (International Center for Diffraction Data) files of different oxide phases. Most of the rings could be indexed consistently based on either the rutile (TiO_2) or the alumina (Al_2O_3, corundum, syn) phases. Thus the rings corresponding to (012) and (113) planes of alumina have been marked by an asterix while the remaining (110), (101) and (211) planes arise from the rutile phase.

Fig. 3 shows a similar study that has been conducted on layer 2 consisting of nanoscale equiaxed grains as shown in the bright-field TEM image in Fig. 3(a). From this figure the average grain size can be estimated as 50-100 nm. A selected area diffraction pattern for this layer is shown as an inset in Fig. 3(a). Based on ICDD files these rings could be consistently indexed as either α-Ti or rutile (TiO_2) phases, indicating that this layer consists of a two phase mixture. The rings for α-Ti could be indexed as the (11-20) and (10-10) planes while the rings for rutile could be indexed to (211), (210) and (101) planes. It should be noted that the intensity of the reflections that are coming from rutile is much lesser than what was obtained in case of layer 1. Since both the diffraction patterns were obtained with the same SAD aperture size, this suggests that the volume fraction of rutile is much lower in layer 2 as compared to layer 1. Also, there seems to be a six fold symmetry in the sections of the rings corresponding to the hexagonal closed packed α-Ti phase. This indicates the presence of a texture within the equiaxed α grains, which is the subject of further investigation. Fig. 3(b) shows a bright field TEM image of layer 2 where one such α grain (dark grain in the center) is in diffracting condition. The SAD pattern obtained from the same precipitate is shown as

an inset in the same figure and can be consistently indexed as the [10-10] α zone axis. The equiaxed morphology of the α grains in this region is clearly evident from the above analyses. Though it seems that the entire layer 2 comprises of a two phase mixture of α-Ti or rutile (TiO_2) phases, it cannot be stated with certainty that no β phase is present in this layer. However, the electron diffraction results do not exhibit any clear evidence for the presence of the β phase within this layer.

Fig. 4(a) is a bright-field TEM image, showing the microstructural transition from layer 2 (equiaxed α + rutile) to layer 3 going from left to right within this image. Thus, while the equiaxed morphology of the fine scale α grains is clearly visible on the left side, the region on the right exhibits a more plate- or lath-like morphology of α phase. Additionally, a substantial increase in the volume fraction of β is also visible within this layer 3. Fig. 4(b) is a bright-field TEM image showing the transition from layer 3 to layer 4. Thus, from left to right in this figure, a change in the size scale (from ~1μm to > 2μm) and nucleation density of α laths is clearly visible. Again, as observed in Fig. 4(a), the β volume fraction appears to be larger on the right side of Fig. 4(b) as compared to the left side. The microstructural changes in Figs. 4(a) and 4(b) are quite apparent and since prior to oxidation the microstructure of this alloy consisted of a compositionally uniform single β phase, these microstructural changes can be solely attributed to the oxygen concentration gradient from layer 2 through layer 4. Further investigation on the exact role of oxygen on the nucleation density and morphology of α precipitates is currently underway.

In this investigation, the influence of oxygen diffusion on the microstructure and hardness of oxygen-enriched regions in an oxidized β-Ti alloy has been investigated. Overall the observations can be summarized as follows:

1. Below the oxide layer (layer 1) lies the oxygen enriched case layer (layer 2) that comprises of a two-phase mixture of rutile (TiO2) and nanometer scale equiaxed α grains.
2. Below this case layer there is gradual but distinct change in the size-scale and nucleation density of lath-like α precipitates (from layer 3 to layer 4) due to the oxygen gradient present in these regions.
3. These microstructural changes have a significant influence on the mechanical properties of these layers, as evident from the nano-indentation test results.

References

[1] R. Boyer, G. Welsch, E.W. Collings (Eds.), Materials Properties Handbook: Titanium Alloys, ASM Intl, Materials Park, OH, 1994

[2] Advanced Aerospace Alloys, Materials Eng., August 1991, p. 26

[3] R. Boyer, *Mat. Sci. and Eng*. A213, 103 (1996).

[4] V.V. Shevel'kov, *Translated from Metallovedenie i Termicheskaya Obrabotke Metallov*, **8**, 33 (1992).

[5] J.C Fanning, *Jour. Mat. Eng. Perf.,* **14**(6), 788 (2005).

[6] P.J. Bania, and W. M Parris., TDA Intl. presentation, 1990, Orlando, FL.

[7] R.W. Schutz, *JOM*, **46**(7), 24 (1994).

[8] N.Agarwal, A. Bhattarcharjee, P. Ghosal, T.K. Nandy and P.K.Sagar, *Trans. Indian Inst. of Metals*, **61**(5), 419 (2008)

[9] X.Huang, J.Cuddy, N. Goel, N.L.Richards, *JMEPEG* **3**, 560 (1994).

[10] Xu Guangjun, Yang Gaiying and Zhu Jing, *Rare Metals* **18**(3), (1999).

[11] T.A.Wallace, K.E.Wiedemann a*nd R.K.Clark*, *Titanium 92, Science and Technology* (1993).

[12] Y.G. Li, P.A. Blenkinsop, M.H. Loretto, D. Rugg and W. Voice, *Acta. Mater.*, **47**(10), 2889 (1999).

[13] M.A.Imam and C.R.Feng, *Advances in the science and technology of titanium alloy processing, The Minerals, Metals & Materials society* (1997).

[14] A.M.Chaze, C.Coddet, *Jour. of Mater. Sci.* **22** 1206 (1987).

Figure captions

Figure 1 (a) Secondary electron image of oxidized Beta21s cross-sectional sample showing the oxide layer along with variation in the size-scale and nucleation density of α precipitates. Superimposed on it is a plot showing the variation of oxygen counts with distance from the top surface. (b) High magnification secondary electron image of the same sample showing two different rows of nanoindentations. Superimposed on it is a plot showing the hardness values obtained from these indents as a function of distance from the oxide-alloy interface.

Figure 2 (a) Scanning transmission electron microscopy (STEM) image showing the change in microstructure, starting from the oxide layer on the top to about 15 μm into the specimen.. (b) Bright field TEM image of the oxide layer showing large number of nanocrystalline grains. Inset shows lower left quadrant of the corresponding SAD pattern analyzed to identify the oxide phases.

Figure 3 (a) Bright field TEM image of the region having nanoscale grains of equiaxed α along with a minute concentration of oxides. Inset shows the corresponding SAD pattern with multiple rings obtained from α-Ti and rutile (TiO_2). (b) Bright field TEM image where one α precipitate (dark grain in the center) is in diffracting condition. Inset shows an SAD pattern obtained from the same precipitate.

Figure 4 Bright field TEM images showing the transition region from (a) equiaxed α precipitates (layer 2) to fine α laths (layer 3) and (b) fine scale α laths (layer 3) to larger α laths (layer 4).

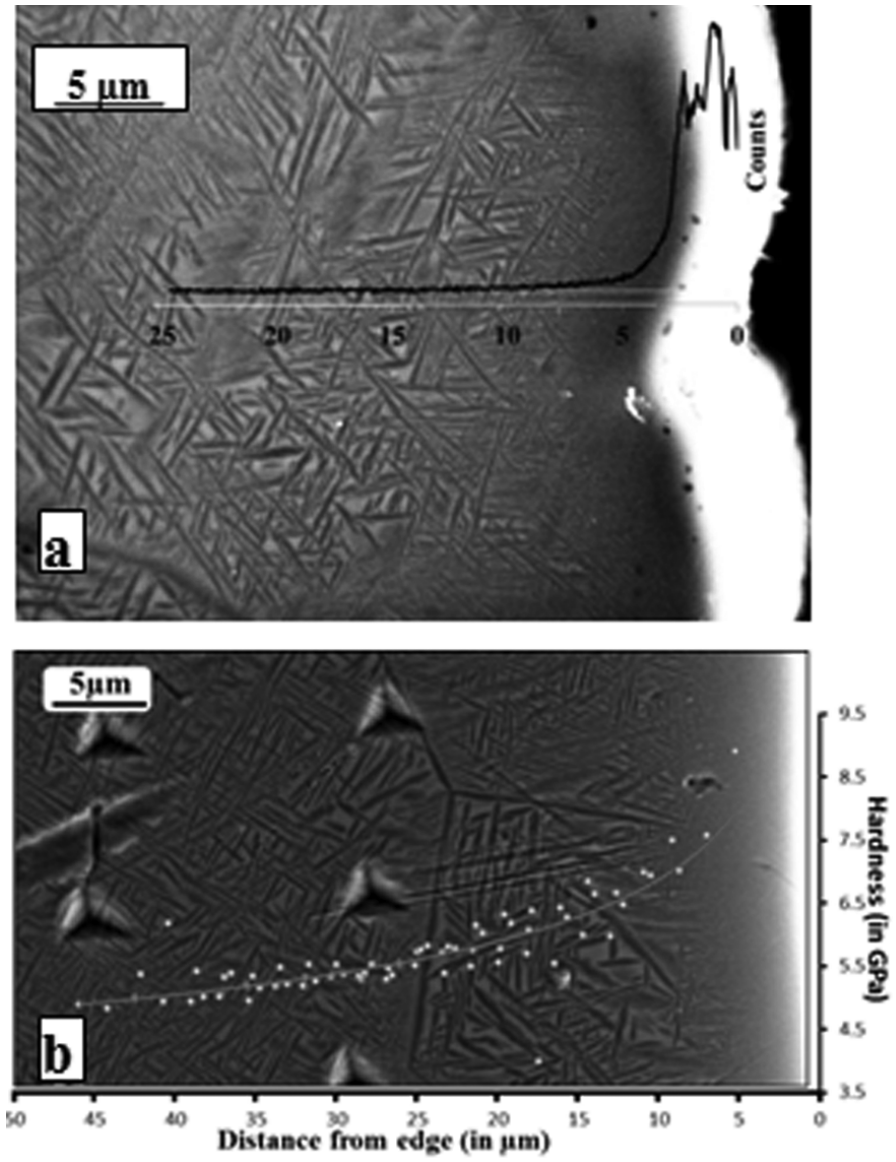

Fig. 1.

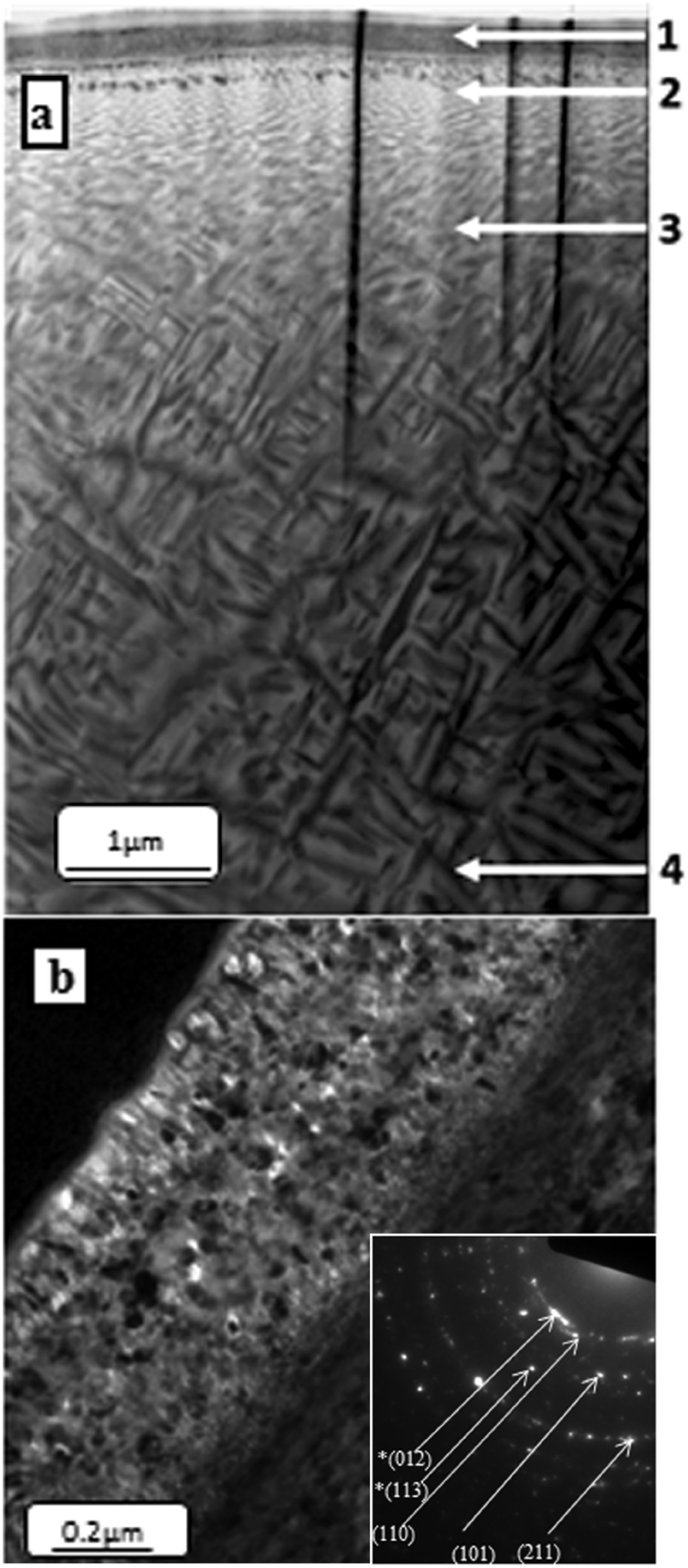

Fig. 2.

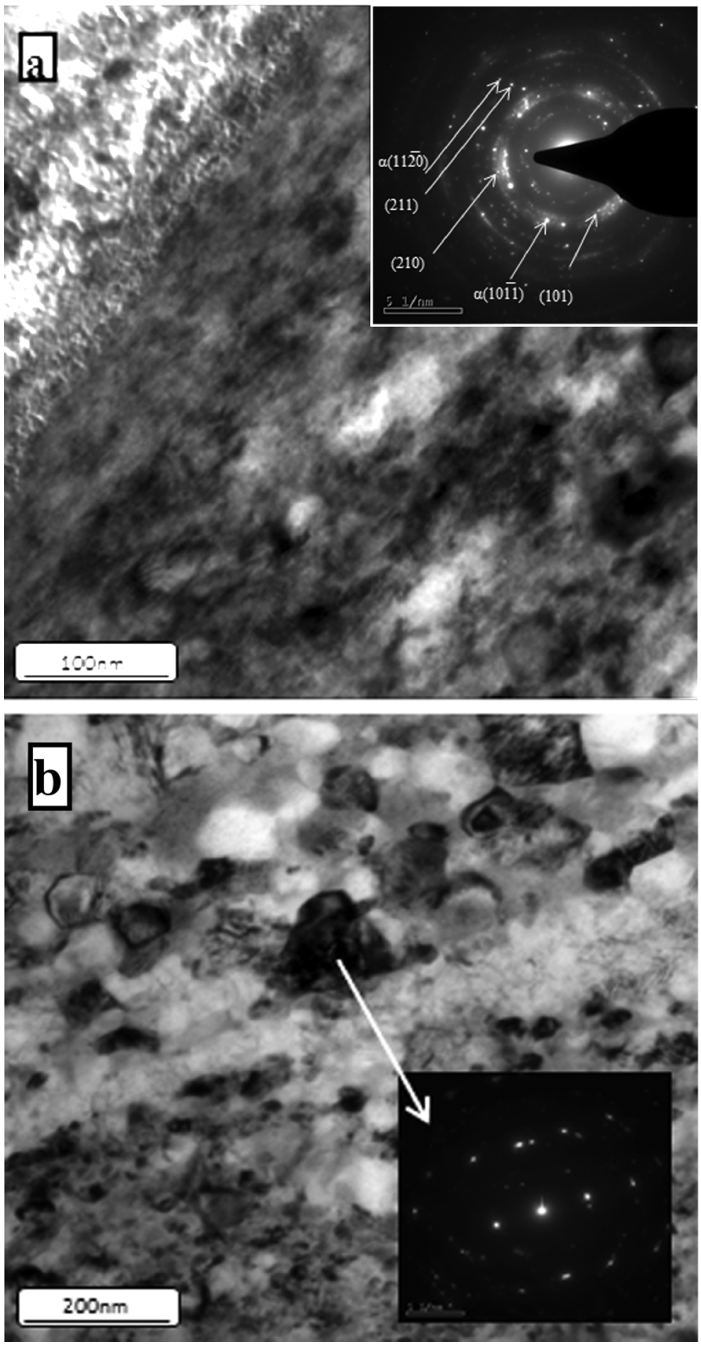

Fig. 3

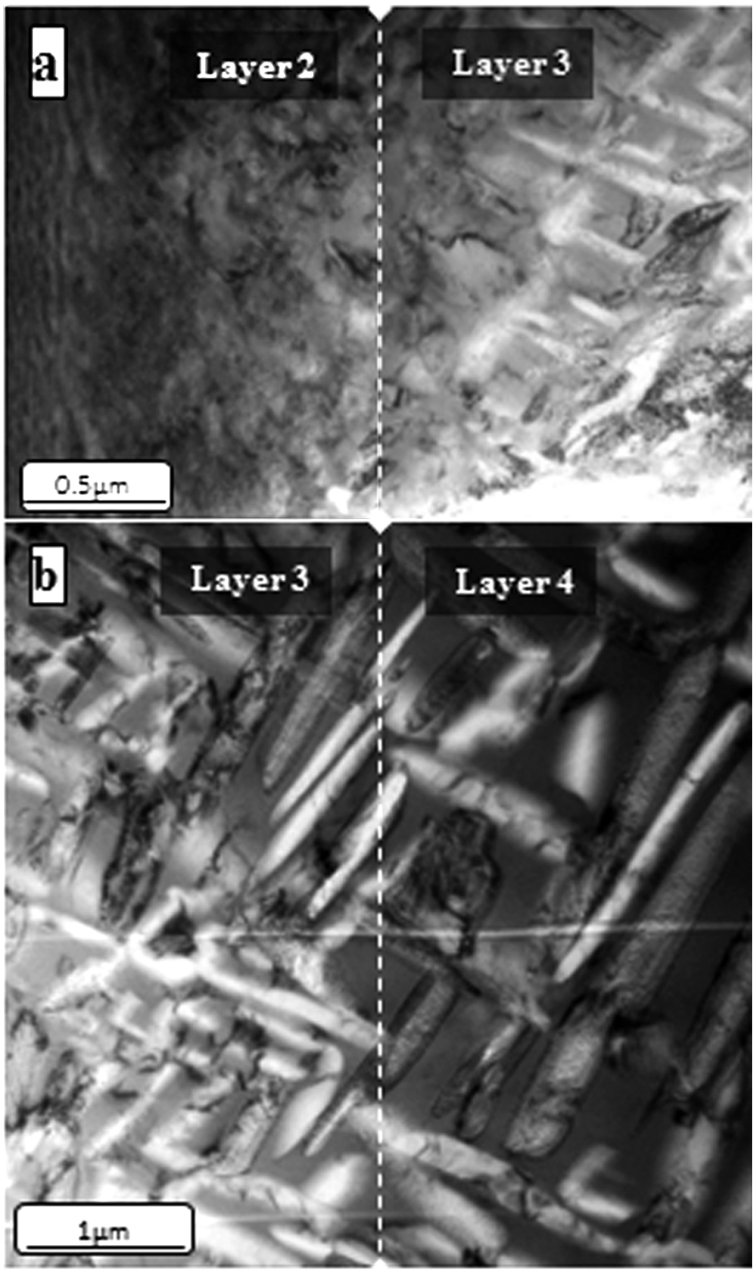

Fig. 4